Chemical Science

ROYAL SOCIETY OF CHEMISTRY

EDGE ARTICLE

View Article Online
View Journal | View Issue

Cite this: *Chem. Sci.*, 2025, **16**, 21633

All publication charges for this article have been paid for by the Royal Society of Chemistry

Received 3rd July 2025
Accepted 12th October 2025

DOI: 10.1039/d5sc04922a

rsc.li/chemical-science

Fibrous intrinsically zeolitic pickering emulsifier

Shuangjia Wang,[a] Xiaoliang Huang,[b] Fei Ma,[c] Wenjun Jiang,[a] Zhifeng Zeng,[a] Yang Zhang,[a] Yuyan Yao[a] and Jiuxing Jiang *[ac]

The intrinsic amphiphilicity that enables grafting-free zeolite Pickering emulsification has been reported previously by us. However, only one type of anisotropic form, *i.e.*, layer morphology, is reported. In this study, we successfully synthesized another anisotropic form, *i.e.*, fibrous zeolitic **TON**, with high crystallinity and dispersion. Furthermore, we defined the anisotropic index to evaluate the anisotropy of the zeolite particles. The high anisotropy (anisotropic index = 17.7) and dispersion result in an amphiphilicity that facilitates the stabilization of the emulsion by the bare zeolite. To our surprise, the emulsion exhibits a very stable state in a basic environment, in contrast with the previous emulsion that is stable at low and medium pH (the Brønsted acid site will be quenched under alkaline conditions). In addition to the anisotropy and dispersion, the zeta potential of fibrous particles plays important roles regardless of the counterpart cations present in the zeolite (H^+, Na^+, or a mixture). This feature indicates their applicability in catalytic reactions under alkaline conditions. Finally, Pd nanoparticles are further deposited on zeolites, leading to a catalyst for the bromobenzene/water biphasic Suzuki–Miyaura C–C coupling. Pd/**TON** acts as not only an emulsifier but also a catalyst in the reaction, making Pd/**TON** a Pickering interfacial catalyst (PIC). The advantages of PICs are: (1) almost 100% product yield is achieved within 20 min; and (2) easy recovery of the product just by filtration or centrifugation, which makes the reaction system environmentally friendly.

Introduction

An emulsion is a homogeneous system consisting of droplets of the dispersed phase dispersed within the continuous phase.[1] Pickering emulsions represent a class of emulsions formulated with ultrafine solid particles or solid colloidal particles, serving as alternatives to conventional surfactants for emulsification.[2] These systems exhibit notable advantages, including enhanced stability, ease of control, environmental sustainability, and cost-effectiveness.[3] Consequently, they have found extensive applications across diverse sectors such as petroleum engineering,[4] water treatment processes,[5] cosmetics formulation,[6] food technology,[7] pharmaceuticals,[8,9] and materials science.[10]

The primary characteristic of solid particles that facilitate the formation of stable Pickering emulsions lies in their dual wetting properties, unique morphology (including size and shape), and concentration levels.[11,12] Among various types of solid particles, a significant proportion of inorganic solids can effectively function as Pickering emulsifiers. Among these, solid nanoballs, nanorods, and nanoplates are extensively utilized for the stabilization of Pickering emulsions. The self-assembly of these solid particles at the fluid interface enhances the stability of the Pickering emulsion.[13] However, previous studies have shown that the self-assembly structure of nanoscale spherical solid particles formed at the oil–water interface is mainly controlled by direct interactions between particles, while capillary interactions seem to dominate for non-spherical particles.[14] There is a clear difference between anisotropic particles, including a lowering of the percolation threshold and an expansion of the range of coverage density achieved through random blocking.[15] Highly anisotropic nanoparticles can significantly enhance the viscoelastic properties of the oil–water interface while concurrently diminishing the interfacial tension between these two phases.[16]

The catalytic system in which solid particles at the liquid/liquid interface of Pickering emulsions can act as both emulsifiers and catalysts is called the Pickering interfacial catalytic (PIC) system.[17] The solid particles are highly dispersed at the liquid/liquid interface, which makes the Pickering emulsion more stable and allows for a significant increase in catalytic reaction efficiency.[18,19] Therefore, particles with moderate wettability and amphiphilicity are expected to stabilize emulsions. However, most heterogeneous catalysts, including zeolites, are hydrophilic and need grafting modification to improve this weakness.[5,20–23] Although the final materials could

[a]*School of Chemistry, MOE Key Laboratory of Bioinorganic and Synthetic Chemistry, Sun Yat-sen University, Guangzhou 510006, P. R. China. E-mail: jiangjiux@mail.sysu.edu.cn*

[b]*Lanzhou Petrochemical Research Center, Petrochemical Research Institute, PetroChina, Lanzhou 730060, China*

[c]*Jiangxi Provincial Key Laboratory of Low-Carbon Solid Waste Recycling Technology, School of Geography and Environmental Engineering, Gannan Normal University, Ganzhou 341000, China*

emulsify the biphasic system, the amphiphilicity is extrinsic, *i.e.* not naturally born. Most inorganic solid particles, such as clay minerals, exhibit limited ability (intrinsic amphiphilicity) for stable emulsion formation without any modification or treatment.[24] Direct emulsification leads to inadequate emulsion stability or necessitates higher concentrations of solid particles. In many cases, surface grafting of organosilanes or co-emulsification with organic surfactant molecules is required. This conclusion is also true for the zeolite before our previous work. Table S1 shows a comparison between this work and the previous preparation of emulsions with inorganic solid particles.

We previously demonstrated a grafting-free MWW layer zeolite that could emulsify a water/oil system.[25] The intrinsic amphiphilicity could be attributed to the ABCD criteria: (A) anisotropy; (B) Brønsted acid; (C) covalency; (D) dispersity. On one side, besides the layer type of anisotropy, will fibrous anisotropy work? On the other side, the genesis of amphiphilicity relies on strong Brønsted acid sites.[26] This means the amphiphilicity will be lost at high pH. Can the zeolite stabilize the emulsion in alkaline media? More importantly, even though anisotropy is a well-known concept that describes the particle morphology divided from a cube/sphere, there is no literature providing a quantitative definition to the best of our knowledge. Therefore, all the issues should be addressed in the research work.

In this work, a fibrous zeolite, **TON** intrinsic Pickering emulsifier, that emulsifies oil–water mixtures without any surface modification is reported. By modifying the synthesis formula in the literature,[27] we obtained a **TON** zeolite with high anisotropy (anisotropic index = 17.7) and dispersion, which is responsible for the intrinsic amphiphilicity. Subsequently, the Pd-loaded **TON** zeolite successfully stabilized the bromobenzene/water emulsion system and catalyzed the Suzuki–Miyaura reaction in the Pickering emulsion system, exhibiting outstanding catalytic performance (Fig. 1).

Results and discussion

A series of samples were prepared with gel compositions: 0.03 Na_2O/0.004 Al_2O_3/1.0 SiO_2/0.45 HDA (1,6-hexamethylenediamine)/50 H_2O/*x*TEABr, where x = 0, 0.05, 0.10, 0.15, or 0.20, named **TON**-N or **TON**-*x*T. The XRD patterns of the samples are shown in Fig. 2a and SEM images in Fig. 2b–f. Firstly, we attempt the synthesis with HDA only, and **TON**-N is obtained as a pure phase[28] with a hollow sphere interwoven by

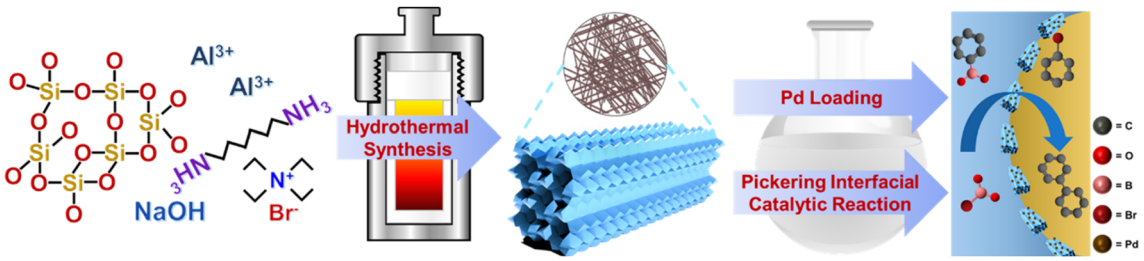

Fig. 1 Experimental design of the sample preparation and PIC catalytic reaction.

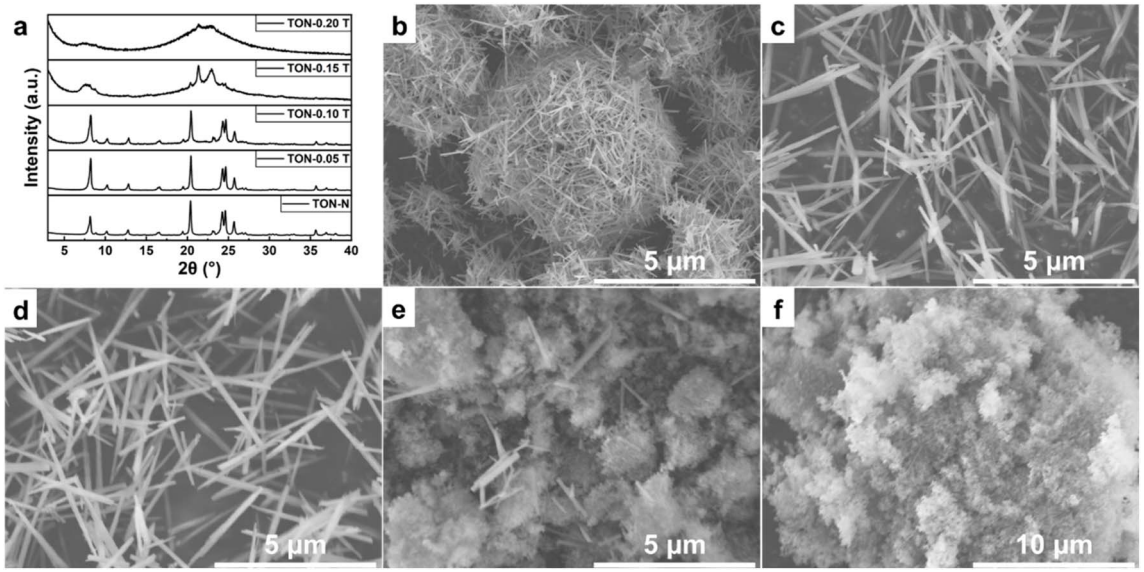

Fig. 2 (a) XRD patterns of **TON**-N and **TON**-*x*T (gel compositions: 0.03 Na_2O/0.004 Al_2O_3/1.0 SiO_2/0.45 HDA/50 H_2O/*x* TEABr). SEM images of (b) **TON**-N, (c) **TON**-0.05T, (d) **TON**-0.10T, (e) **TON**-0.15T and (f) **TON**-0.20T.

zeolite needles (diameter ranging from 180–250 nm and an average length of 2 μm). When tetraethylammonium bromide (TEABr) is introduced with $x = 0.05$ and 0.10, the agglomerated fiber spheres gradually transform into highly dispersed nanofibers, accompanied by a significant increase in single crystal length (Fig. 2c and d). However, as the content of TEABr further increases ($x = 0.15$, 0.20), the zeolite crystallinity significantly decreases.

The average particle size dimensions of the samples are: $\bar{a} =$ 152 nm, $\bar{b} =$ 160 nm, and $\bar{c} =$ 3390 nm, according to the orientation displayed in Fig. S1b and c. Based on the statistical data and the definition of A (anisotropic index, eqn (2) in Methods), that gives $A = 17.7$. We posit that an increase in the value of A correlates with enhanced anisotropy of solid particles, which in turn facilitates more favorable conditions for emulsion formation.

The emulsifying properties of **TON**-N and **TON**-0.05T were further investigated by evaluating their capacity to form emulsions in an *n*-tetradecane/water system. As depicted inFig. 3a and b, the dispersion degree of the zeolite significantly influences the formation of an emulsion. **TON**-N produced unstable emulsions with rapid phase separation; the use of **TON**-0.05T, which exhibits a higher level of dispersion, results in stable Pickering emulsions that can persist for extended periods with relatively uniform droplet diameters around 75 μm (Fig. 3c and d). To more precisely define the size of the oil–water interface, specifically the contact area of oil–water phases in the emulsion, we suggest the interfacial area calculation formulas (eqn (3) and (4) of the emulsion as seen in the SI). It is evident that the formation of an emulsion system significantly increases the contact area between solid particles/oil/water systems, thereby accelerating and improving the efficiency of the catalytic reaction.

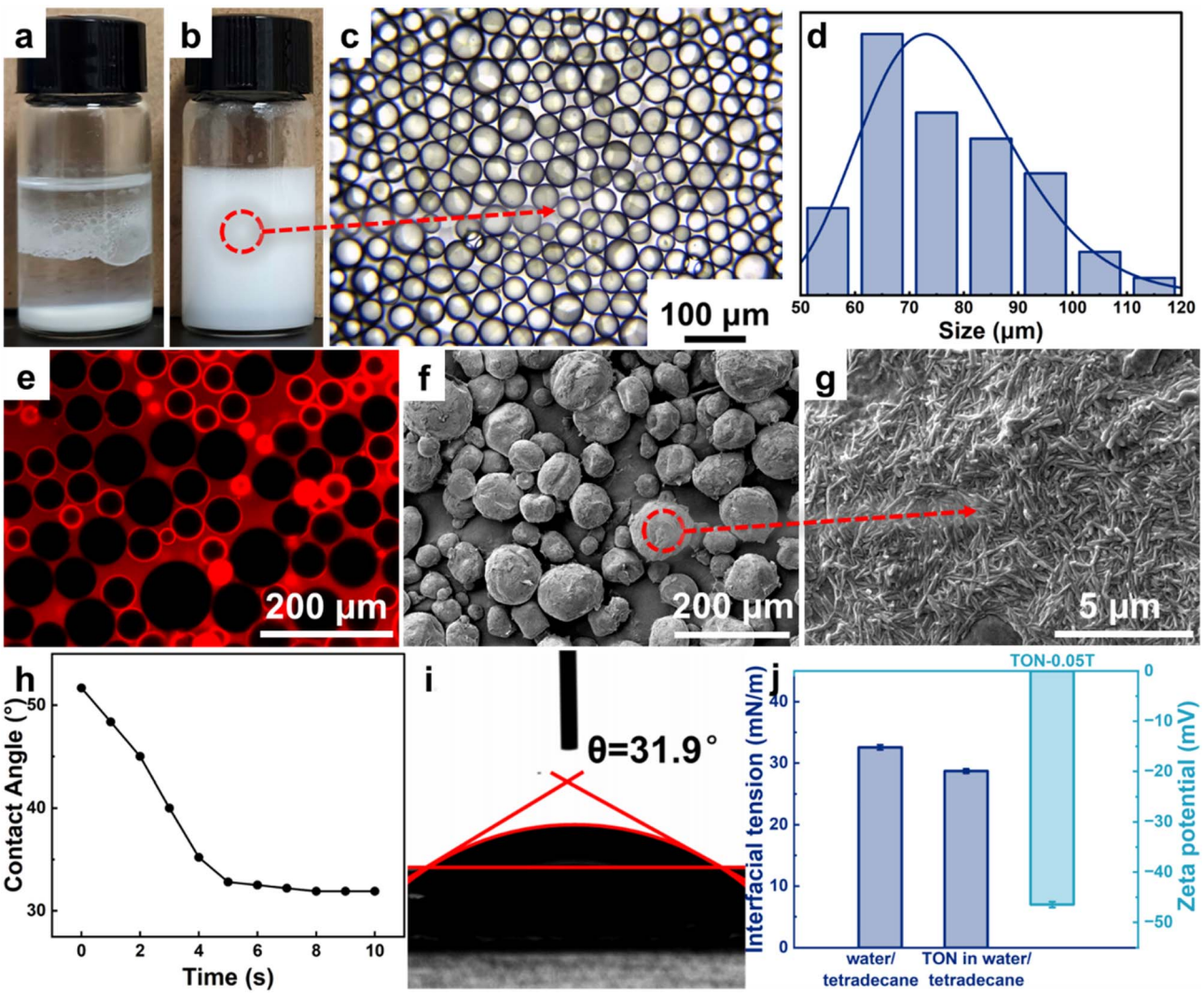

Fig. 3 Photographs and optical microscopy image of tetradecane-in-water emulsions stabilized by 1.0 wt% (a) **TON**-N and (b and c) **TON**-0.05T. (d) The size distribution histogram of a Pickering emulsion stabilized by 0.5 wt% **TON**-0.05T. (e) CLSM image of the tetradecane-in-water emulsion stabilized by Rhodamine B labeled **TON**-0.05T. (f and g) SEM images of a paraffin-in-water emulsion stabilized by 1.0 wt% **TON**-0.05T. (h) Change of the three-phase contact angle of **TON**-0.05T with time. (i) Image of the stable three-phase contact angle of **TON**-0.05T. (j) Water/tetradecane interfacial tension with and without 0.5 wt% **TON**-0.05T and zeta potential of **TON**-0.05T at 25 °C.

To explore the mechanism of Pickering emulsion formation, **TON**-0.05T was stained with Rhodamine B, and the emulsion was visualized with Confocal Laser Scanning Microscopy (CLSM). A bright red circle around the oil droplets and red fluorescence signals in the continuous phase can be observed. These indicate the presence of **TON**-0.05T zeolite fibers plays two roles: (1) wrap up the oil droplets; (2) assemble into a three-dimensional structure within the continuous phase to keep distance between droplets (Fig. 3e); both factors stabilize the emulsion.[29] Due to the liquid state of tetradecane at room temperature, conventional scanning electron microscopy cannot be used to observe tetradecane/water emulsions. Therefore, 52# solid paraffin was employed as a substitute for tetradecane in the oil phase to prepare a Pickering emulsion. As depicted in Fig. 3f, SEM analysis of the solid paraffin emulsion exhibited consistency with microscopic observations, revealing an average oil drop size of approximately 75 μm. By zooming in, a substantial amount of **TON**-0.05T zeolite is uniformly distributed on the surface of the oil droplets (Fig. 3g), effectively preventing coalescence and ensuring the stable existence of the emulsion. These findings highlight the favorable impact of the zeolite's high dispersion on emulsion formation and indicate that the zeolite fiber is an excellent support for Pickering interfacial catalysts. We performed an emulsion stabilization mechanism experiment solely using grafting-free **TON**-0.05T.

To investigate the amphiphilicity of the zeolite, contact angle tests were conducted on **TON**-0.05T zeolite. The hydrophilicity of **TON**-0.05T is evident from the results shown in Fig. 3h, the video image capture method was employed for analysis, and the final stable three-phase contact angle is 31.9° (Fig. 3i),

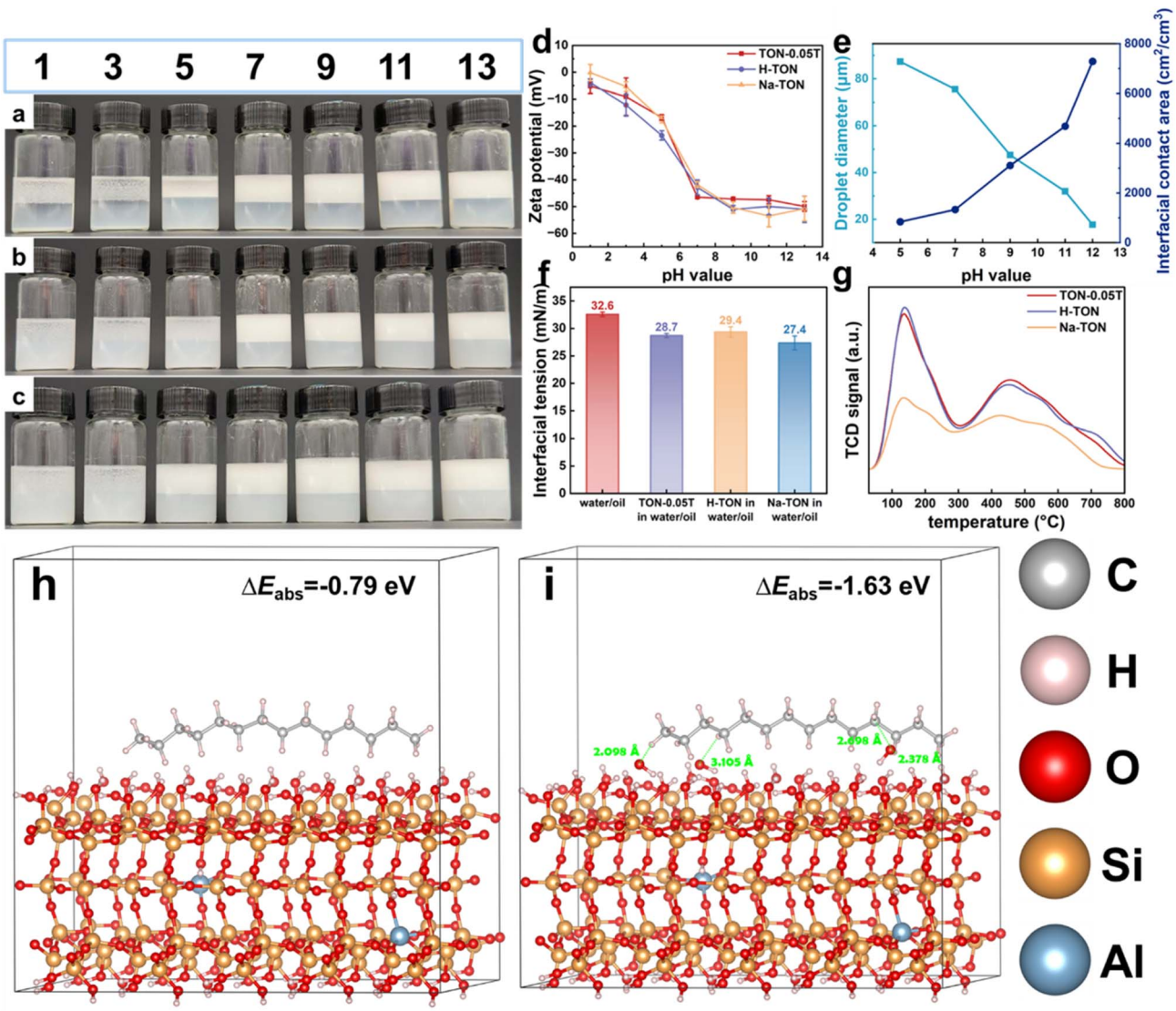

Fig. 4 Photographs of Pickering emulsions prepared from (a) **TON**-0.05T, (b) H-**TON** and (c) Na-**TON** at different pH values (the numbers in the boxes indicate the pH values of the systems). (d) Graph of the variation of zeta potential on the **TON** zeolite with different pH values. (e) Variation diagram of droplet diameters of emulsion and the interfacial contact area between oil and water with pH value. (f) Water/tetradecane interfacial tension with **TON**-0.05T, H-**TON** and Na-**TON** at 25 °C. (g) NH_3-TPD curve profiles of **TON**-0.05T, H-**TON**, and Na-**TON**. All emulsions were observed after 24 h of standing at 25 ± 2 °C. The DFT-optimized adsorption configuration of tetradecane on **TON**: (h) pH = 7, $\Delta E_{abs} = -0.79$ eV; (i) pH = 13, $\Delta E_{abs} = -1.63$ eV.

indicating the hydrophilicity of **TON**-0.05T. At the same time, the interfacial tension of tetradecane–water was decreased slightly with **TON**-0.05T (Fig. 3j), which facilitated emulsion formation. It is generally believed that when the zeta potential value is greater than 30 mV or less than −30 mV, the agglomeration of particles tends to weaken due to the increase of surface charge and the increase of repulsion force between particles. In contrast, when the zeta potential value is in the range of −30 to 30 mV, the solid particles tend to aggregate.[30] At 25 °C, the zeta potential of **TON**-0.05T is −46.5 mV, indicating that zeolite is highly dispersed in water, which is consistent with SEM, which grants it great potential for emulsification.

To gain a more comprehensive understanding of the emulsification ability of **TON** zeolite, we carried out emulsification experiments of **TON**-0.05T, H-**TON**, and Na-**TON** in different pH environments. As can be seen fromFig. 4a–c, poor emulsification ability is shown in an acidic environment, a large amount of demulsification occurs, oil droplets condense rapidly, and zeolite falls off from the oil–water interface. It can be seen from the microscopic images (Fig. S2) of the emulsion that as the pH value of the system increases, the particle size distribution of the emulsion gradually decreases, and the emulsion tends to be more stable.

Concurrently, we also conducted zeta potential tests on **TON**-0.05T, H-**TON**, and Na-**TON** zeolites in different pH environments (Fig. 4d). It was found that in acidic environments, the zeta potential tended to approach the isoelectric point (0 mV), which would make the zeolite particles more prone to agglomeration and thus less conducive to emulsification. In contrast, in neutral or alkaline environments, the zeta potential was always less than −40 mV, making the zeolite particles exhibit a more dispersed state in the dispersed phase. This result also corresponds to the emulsification phenomenon. Based on the formulas in eqn (3) and (4), the oil–water interface contact area of the emulsion stabilized by **TON**-0.05T at different pH values was calculated (Fig. 4e). It can be seen that the contact area gradually increases with the increase of pH value. At pH = 13, the contact area reached an astonishing 7285.9 cm^2 cm^{-3}. The same situation occurred in Na-**TON** zeolite and H-**TON** zeolite. This is probably because the presence of H^+ in an acidic environment leads to the protonation of the silico-hydroxyl group (Si-OH) of the zeolite, which makes the zeolite more hydrophilic and reduces the emulsification performance. In contrast, in an alkaline environment, the emulsion layer exhibits a very stable state with almost no zeolite loss. At the same time, the interfacial tension of tetradecane–water was decreased slightly with **TON**-0.05T, H-**TON** and Na-**TON** (Fig. 4f), which facilitated emulsion formation. Therefore, this zeolite is particularly well-suited for emulsion preparation and catalysis in alkaline media.

The NH_3-TPD curves are presented in Fig. 4g; the curves of all samples exhibit two NH_3 desorption peaks in the low-temperature region of 150–300 °C (T_{dL}) and the high-temperature region of 300–500 °C (T_{dH}), which suggests the presence of weak and strong acid sites, respectively. The coordination environment of Si and Al species was investigated using solid-state NMR. Only an intense peak around 55 ppm was observed in ^{27}Al MAS NMR spectra (Fig. S3a), which can be assigned to the tetrahedral coordinated Al in the framework.[31] For the ^{29}Si MAS NMR spectra shown in Fig. S3b, five peaks at −114, −113, −111, −110, and −105 ppm were deconvoluted. The first four peaks were associated with Si(0Al) units, while that at −105 ppm corresponded to Si(1Al) units;[32] the results are presented in Table S2. The Si/Al atomic ratio of **TON**-0.05T from the ^{29}Si MAS NMR spectra[33] is 55.8 (calculation procedure as seen in the SI), which is consistent with the result obtained from the ICP elemental analysis in Table S3. A higher Si/Al ratio will make zeolite possess a certain degree of lipophilicity, thereby further enhancing its emulsifying ability.

Therefore, we are trying to rationalize the emulsification mechanism of fibrous morphology compared with the layer one. Firstly, due to its strong anisotropy (same as that of the layer one), **TON**-0.05T exhibits a fibrous morphology with an anisotropic index as high as $A = 17.7$. Secondly, high dispersion (same as that of the layer one) avoids mutual interference to properly distribute on the oil-water interface. Thirdly, the high Si/Al ratio endows the zeolite with a certain lipophilic character (higher than that of the layer one, MWW Si/Al ∼10). Finally, the zeta potential (rather than the Brønsted acid) is responsible for the switch of emulsification. Hence, a deeper understanding is necessary to reach a comprehensive theory for both layer and fibrous morphology. Therefore, density functional theory (DFT) calculations were employed to investigate the adsorption mechanism of the **TON** zeolite toward a model oil (tetradecane) under neutral (pH = 7) and alkaline (pH = 13) conditions. In the neutral system (pH = 7), no explicit hydroxide ions (OH^-) were introduced (Fig. S4a). In contrast, under the alkaline conditions (pH = 13), three OH^- ions were explicitly placed on the surface of the **TON** zeolite to simulate the high-pH environment (Fig. S4b). Following DFT geometry optimization, these OH^- ions were found to form multiple hydrogen bonding interactions with the zeolite framework. Subsequently, the adsorption behavior of tetradecane was compared between the two systems. The calculated adsorption energy of tetradecane on the **TON** surface at pH = 7 was −0.79 eV (Fig. 4h). In the pH = 13 system, the surface-located OH^- ions exhibited a synergistic effect on tetradecane adsorption, effectively stabilizing the hydrocarbon molecule and enhancing the overall adsorption affinity, as evidenced by the significantly increased adsorption energy of −1.63 eV (Fig. 4i). These theoretical findings, in conjunction with previous experimental studies, support the consistency of the observed adsorption trends with fundamental physicochemical principles, thereby providing a rational theoretical basis that complements and reinforces existing experimental results.

Based on the above, a simple surface impregnation method was used to deposit Pd nanoparticles on the surface of **TON**-0.05T. According to ICP data analysis in Table S3, the content of Pd nanoparticles is 0.91 wt%. Fig. 5a shows the X-ray diffraction (XRD) pattern of raw and Pd-impregnated zeolites. No peaks corresponding to the palladium species can be identified in the XRD pattern. This phenomenon may be due to the small size of Pd nanoparticles and the wide dispersion of Pd species in **TON**-0.05T zeolite. This result also confirms that the skeleton topology of zeolite can still be preserved intact after Pd

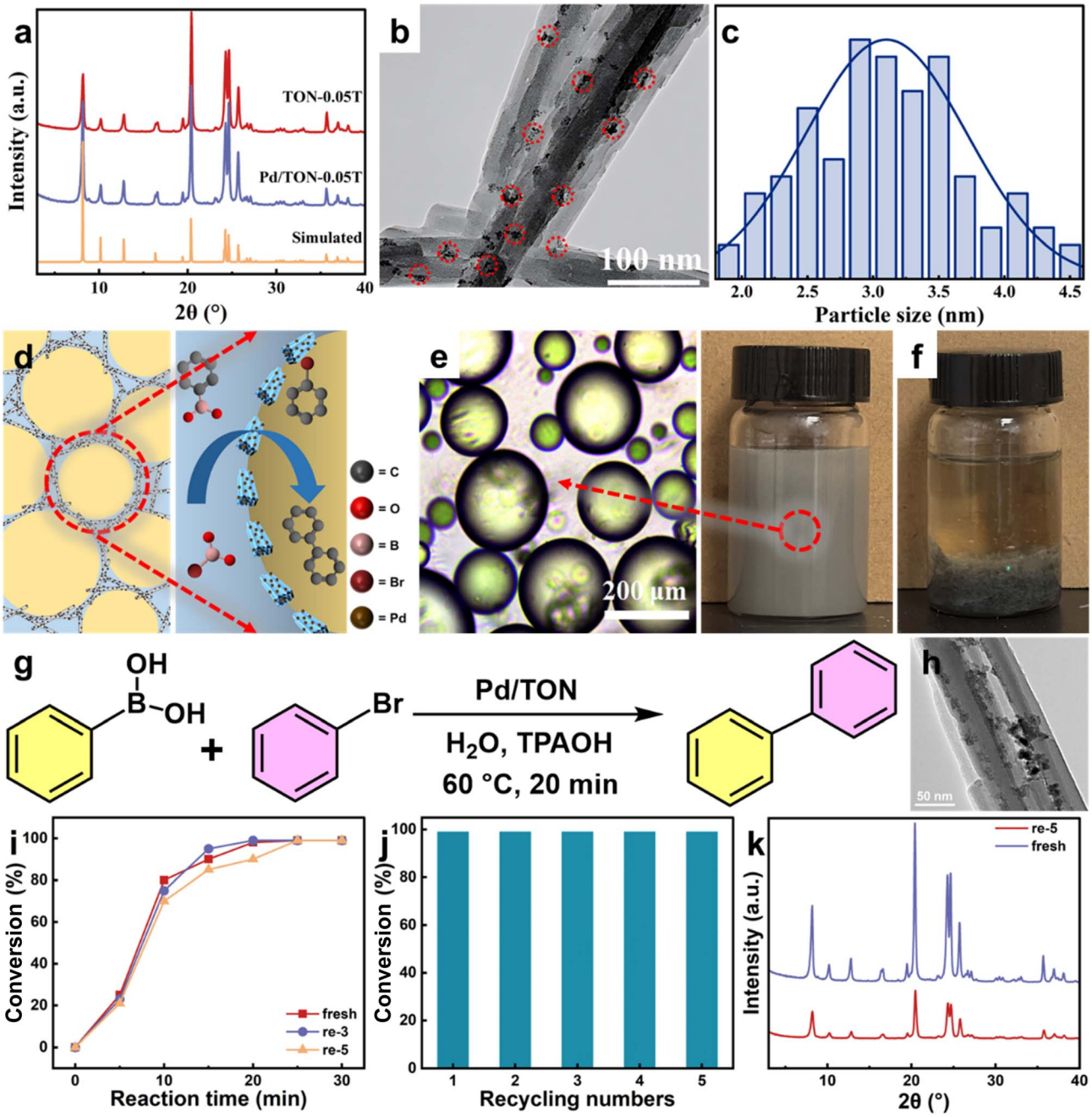

Fig. 5 (a) XRD patterns of **TON**-0.05T and Pd/**TON**-0.05T, (b) TEM image of Pd/**TON**-0.05T, showing the highly dispersed Pd NPs on the support, (c) Pd NP size distribution of **TON**-0.05T. (d) Scheme for the Suzuki–Miyaura reaction catalyzed by Pd/**TON**-0.05T. (e) Optical microscopy and photograph images of the mixture of phenylboronic acid in water and bromobenzene in the presence of Pd/**TON**-0.05T (successfully emulsified). (f) Photograph of the reaction product. (g) The scheme of the catalytic reaction. (h) TEM image of Pd/**TON**-0.05T reacted for 5 cycles. (i) Time course change in the conversion of bromobenzene over Pd/**TON**-0.05T. (j) Durability test of Pd/**TON**-0.05T in the Suzuki–Miyaura reaction. (k) XRD patterns of fresh and reacted (for 5 cycles) Pd/**TON**-0.05T.

impregnation treatment for a long time. Subsequently, TEM characterization was performed on the prepared solid catalyst, as shown in Fig. 5b. The results show that Pd nanoparticles are uniformly deposited on the fibrous surface of **TON**-0.05T, and the size of Pd nanoparticles on the zeolite surface is about 3.2 nm (Fig. 5c). To evaluate whether the emulsification capability of **TON** was significantly affected by Pd loading, the contact angle and oil–water interfacial tension of Pd/**TON**-0.05T were measured using the same characterization methods employed for **TON**-0.05T. As shown in Fig. S5a, the final contact angle of Pd/**TON**-0.05T was determined to be 32.5°. Upon the introduction of Pd/**TON**-0.05T, the interfacial tension between tetradecane and water decreased, reaching a final value of 28.6 mN m^{-1}. Moreover, the zeta potential remained similar to that of the Pd-free **TON** sample, with a measured value of −45.1 mV (Fig. S5b). These results indicate that the incorporation of Pd

does not significantly alter the emulsification performance of **TON** toward oil and water. Further experimental outcomes consistently support this conclusion.

As shown in Fig. 5d, Pd/**TON**-0.05T is adsorbed at the oil–water interface to catalyze the Suzuki–Miyaura reaction. In this reaction, bromobenzene and phenylboric acid aqueous solutions were violently stirred under the action of a solid catalyst to obtain a Pickering emulsion reaction system (Fig. 5e). After the reaction at 60 °C for 20 minutes, the solid reaction product was obtained after rapid cooling to room temperature (Fig. 5f). After filtering and separating the reaction products, the solid catalyst can be recovered for the next catalytic experiment. As can be seen from Fig. 5i, the conversion rate of reaction products reached 99% when the reaction time was 30 minutes, and the reaction activity of the solid catalyst was still retained after five cycles of testing (Fig. 5j). Upon calculation, the turnover frequency (TOF) values for Pd/**TON**-0.05T reached up to 702 h^{-1} (Table S4), indicating the potent reactivity of the zeolite-supported palladium catalyst. In addition, XRD patterns and TEM images of the solid catalyst showed no significant changes after five cycles (Fig. 5k and h). It can be seen from the above experimental data that Pd/**TON**-0.05T has good emulsification performance and catalytic capacity, and can catalyze the Suzuki–Miyaura reaction efficiently and can be reused. As shown in Table S4, under similar conditions, our Pd/**TON**-0.05T catalyst exhibits superior catalytic activity compared with other supported catalysts. This comparison endeavors to highlight the differential catalytic performance, efficiency, and stability of various catalysts under similar reaction conditions.

Conclusions

In summary, the successful preparation of stable Pickering emulsions is attributed to the intrinsic amphiphilicity of **TON**-0.05T zeolite. This reliable amphiphilicity is obtained through the combined effects of the highly anisotropic morphology of the zeolite, its high dispersion stability, the high Si/Al ratio, and the high absolute value of zeta potential at high pH. Finally, the **TON**-0.05T zeolite loaded with Pd successfully stabilized the bromobenzene/phenylboric acid aqueous solution emulsion system and demonstrated superior conversion rates for interfacial catalytic reactions.

Using organic reactions in the aqueous phase, we have demonstrated that the catalyst exhibits significant activity at the interface between the reactants and water, and can be easily separated from the reaction mixture. This novel catalyst provides a method to reduce the harmful surfactants and environmentally unfriendly organic solvents generated during processing. These results indicate that zeolite-based Pickering interface catalysts have great potential as high-performance sustainable chemical catalysts.

Author contributions

S. W. and J. J. carried out experiments on zeolite design and characterization, product identification and quantification, and determination of the reaction pathway. X. H. and F. M. helped with experiments on product characterization and catalyst synthesis. W. J., Z. Z., Y. Z. and Y. Y. helped with catalyst synthesis and characterization, and experiments to understand the reaction mechanism. J. J. conceptualized and oversaw the study. S. W. and J. J. co-wrote the paper.

Conflicts of interest

J. X. J., S. J. W. and Z. F. Z. have filed a patent on the preparation and application of PIC catalysts. The remaining authors declare no competing interest.

Data availability

All data are available in the main text and the supplementary information (SI) or available from the authors upon reasonable request. Supplementary information is available. See DOI: **https://doi.org/10.1039/d5sc04922a**.

Acknowledgements

We acknowledge the financial support by the National Natural Science Foundation of China (No. 22372200), Talent Work Group of the Jiangxi Provincial Committee of China (No. jxsq2023102006), and Guangdong Provincial Department of Science and Technology (No. 2021B1212050005).

Notes and references

1 B. P. Binks, Particles as surfactants—similarities and differences, *Curr. Opin. Colloid Interface Sci.*, 2002, **7**, 21–41.
2 D. Gonzalez Ortiz, C. Pochat-Bohatier, J. Cambedouzou, M. Bechelany and P. Miele, Current Trends in Pickering Emulsions: Particle Morphology and Applications, *Engineering*, 2020, **6**, 468–482.
3 C. Albert, M. Beladjine, N. Tsapis, E. Fattal, F. Agnely and N. Huang, Pickering emulsions: Preparation processes, key parameters governing their properties and potential for pharmaceutical applications, *J. Controlled Release*, 2019, **309**, 302–332.
4 D. Chen, A. Wang, Y. Li, Y. Hou and Z. Wang, Biosurfactant-modified palygorskite clay as solid-stabilizers for effective oil spill dispersion, *Chemosphere*, 2019, **226**, 1–7.
5 S. Wang, Y. Shen, X. Chen, L. Dong, H. Yu, M. Bao and Y. Li, Cationic surfactant-modified palygorskite particles as effective stabilizer for Pickering emulsion gel formation, *Appl. Clay Sci.*, 2022, **219**, 106439.
6 L. Cao, W. Xie, H. Cui, Z. Xiong, Y. Tang, X. Zhang and Y. Feng, Fibrous Clays in Dermopharmaceutical and Cosmetic Applications: Traditional and Emerging Perspectives, *Int. J. Pharm.*, 2022, **625**, 122097.
7 C. Linke and S. Drusch, Pickering emulsions in foods - opportunities and limitations, *Crit. Rev. Food Sci. Nutr.*, 2018, **58**, 1971–1985.
8 L. E. Low, L. T.-H. Tan, B.-H. Goh, B. T. Tey, B. H. Ong and S. Y. Tang, Magnetic cellulose nanocrystal stabilized Pickering emulsions for enhanced bioactive release and

human colon cancer therapy, *Int. J. Biol. Macromol.*, 2019, **127**, 76–84.
9 X. Pu, R. Liu, Y. Xie, C. Yang, J. Chen, B. Guo, C.-X. Zhao, P. Zhao, J. Ruan, F. Ye, D. A. Weitz and D. Chen, One-step preparation of biocompatible amphiphilic dimer nanoparticles with tunable particle morphology and surface property for interface stabilization and drug delivery, *Chin. Chem. Lett.*, 2025, **36**, 109820.
10 T. Lu, Y. Zhu, W. Wang and A. Wang, Controllable fabrication of hierarchically porous adsorbent via natural particles stabilized Pickering medium internal phase emulsion for high-efficiency removal of Rb+ and Cs+, *J. Cleaner Prod.*, 2020, **277**, 124092.
11 E. Dickinson, Use of nanoparticles and microparticles in the formation and stabilization of food emulsions, *Trends Food Sci. Technol.*, 2012, **24**, 4–12.
12 W. Zhang, B. P. Binks, J. Jiang and Z. Cui, Smart Emulsions Stabilized by a Multi-headgroup Surfactant Tolerant to High Concentrations of Acids and Salts, *Angew. Chem., Int. Ed.*, 2023, **62**, e202310743.
13 A. Toor, T. Feng and T. P. Russell, Self-assembly of nanomaterials at fluid interfaces, *Eur. Phys. J. E*, 2016, **39**, 57.
14 I. Kalashnikova, H. Bizot, P. Bertoncini, B. Cathala and I. Capron, Cellulosic nanorods of various aspect ratios for oil in water Pickering emulsions, *Soft Matter*, 2013, **9**, 952–959.
15 A. Donev, I. Cisse, D. Sachs, E. A. Variano, F. H. Stillinger, R. Connelly, S. Torquato and P. M. Chaikin, Improving the Density of Jammed Disordered Packings Using Ellipsoids, *Science*, 2004, **303**, 990–993.
16 J.-M. Jung, D. Z. Gunes and R. Mezzenga, Interfacial Activity and Interfacial Shear Rheology of Native β-Lactoglobulin Monomers and Their Heat-Induced Fibers, *Langmuir*, 2010, **26**, 15366–15375.
17 L. Ni, C. Yu, Q. Wei, D. Liu and J. Qiu, Pickering Emulsion Catalysis: Interfacial Chemistry, Catalyst Design, Challenges, and Perspectives, *Angew. Chem., Int. Ed.*, 2022, **61**, e202115885.
18 M. Pera-Titus, L. Leclercq, J.-M. Clacens, F. De Campo and V. Nardello-Rataj, Pickering Interfacial Catalysis for Biphasic Systems: From Emulsion Design to Green Reactions, *Angew. Chem., Int. Ed.*, 2015, **54**, 2006–2021.
19 Y. Xu, H. Liang, R. Li, Z. Zhang, C. Qin, D. Xu, H. Fan, B. Hou, J. Wang, X. K. Gu and M. Ding, Insights into the Diffusion Behaviors of Water over Hydrophilic/Hydrophobic Catalysts During the Conversion of Syngas to High-Quality Gasoline, *Angew. Chem., Int. Ed.*, 2023, **62**, e202306786.
20 A. Kumar, B. J. Park, F. Tu and D. Lee, Amphiphilic Janus particles at fluid interfaces, *Soft Matter*, 2013, **9**, 6604–6617.
21 M. Xu, J. Jiang, X. Pei, B. Song, Z. Cui and B. P. Binks, Novel Oil-in-Water Emulsions Stabilised by Ionic Surfactant and Similarly Charged Nanoparticles at Very Low Concentrations, *Angew. Chem., Int. Ed.*, 2018, **57**, 7738–7742.
22 J. Ma, J. Wang, J. Yuan, X. Liu, Y. Yang and F. Yu, The regulating strategy of hierarchical structure and acidity in zeolites and application of gas adsorption: A review, *Chin. Chem. Lett.*, 2024, **35**, 109693.
23 P. Liu, Q. Wu, Z. Chen and F.-S. Xiao, Recent Advances in the Synthesis of Zeolites from Solid Wastes, *Chem. Res. Chin. Univ.*, 2024, **40**, 646–656.
24 T. Lu, H. Gou, H. Rao and G. Zhao, Recent progress in nanoclay-based Pickering emulsion and applications, *J. Environ. Chem. Eng.*, 2021, **9**, 105941.
25 Z. Zeng, F. Ma, S. Wang, J. Wen, X. Jiang, G. Li, Y. Tong, X. Liu and J. Jiang, Zeolitic Pickering Emulsifier with Intrinsic Amphiphilicity, *J. Am. Chem. Soc.*, 2024, **146**, 9851–9859.
26 S. Bo, T. Wang, T. Lv, H. Wu, Z. Feng, L. Miao, Z. Feng, L. Ren and C. Meng, Rapid Synthesis of Boron-MWW Zeolite Through a Solvent-free Strategy, *Chem. Res. Chin. Univ.*, 2024, **40**, 1245–1255.
27 Q. Wang, H. Shan, L. B. Sim, J. Xie, S. Ye, J. Fu, J. Wang, N. Zhang, J. Zheng and B. Chen, ZSM-22 Synthesized Using Structure-Directing Agents of Different Alkyl Chain Lengths for Controlled n-Hexadecane Hydroisomerizations, *Ind. Eng. Chem. Res.*, 2023, **62**, 11470–11479.
28 G. T. Kokotailo, J. L. Schlenker, F. G. Dwyer and E. W. Valyocsik, The framework topology of ZSM-22: A high silica zeolite, *Zeolites*, 1985, **5**, 349–351.
29 A. D. Dinsmore, M. F. Hsu, M. G. Nikolaides, M. Marquez, A. R. Bausch and D. A. Weitz, Colloidosomes: Selectively Permeable Capsules Composed of Colloidal Particles, *Science*, 2002, **298**, 1006–1009.
30 L. E. Low, S. P. Siva, Y. K. Ho, E. S. Chan and B. T. Tey, Recent advances of characterization techniques for the formation, physical properties and stability of Pickering emulsion, *Adv. Colloid Interface Sci.*, 2020, **277**, 102117.
31 A. Layek, J. Van Loon, M. B. J. Roeffaers and A. V. Kubarev, Correlated super-resolution fluorescence and electron microscopy reveals the catalytically active nanorods within individual H-ZSM-22 zeolite particles, *Catal. Sci. Technol.*, 2019, **9**, 4645–4650.
32 Z. Feng, W. Wang, Y. Wang, X. Bai, X. Su, L. Yang and W. Wu, Hydroisomerization of n-decane over the Pd/ZSM-22 bifunctional catalysts: The effects of dynamic and static crystallization to the zeolite, *Microporous Mesoporous Mater.*, 2019, **274**, 1–8.
33 X. Su, G. Wang, X. Bai, W. Wu, L. Xiao, Y. Fang and J. Zhang, Synthesis of nanosized HZSM-5 zeolites isomorphously substituted by gallium and their catalytic performance in the aromatization, *Chem. Eng. J.*, 2016, **293**, 365–375.